Supplementary Information (SI) for Chemical Communications.
This journal is © The Royal Society of Chemistry 2024

SUPPORTING INFORMATION

Doubly σ- and π-Aromatic Planar Pentacoordinate Boron Polyanions

Williams García-Argote,[ab]† Dumer S. Sacanamboy,[ab]† Alejandro Vasquez-Espinal[c], Diego Inostroza,[d] Luis Leyva-Parra,*[e] Osvaldo Yañez,*[f] and William Tiznado*[a]

[a] *Centro de Química Teórica & Computacional (CQT&C), Facultad de Ciencias Exactas, Departamento de Ciencias Químicas, Universidad Andrés Bello, Avenida República 275, Santiago 837014, Chile.* wtiznado@unab.cl

[b] *Doctorado en Fisicoquímica Molecular, Facultad de Ciencias Exactas, Universidad Andrés Bello, República 275, Santiago 837014, Chile.*

[c] *Química y Farmacia, Facultad de Ciencias de la Salud, Universidad Arturo Prat, Casilla 121, Iquique 1100000, Chile*

[d] *Departamento de Física, Facultad de Ciencias, Universidad de Chile, Ñuñoa, Santiago 7800024, Chile*

[e] *Facultad de Ingeniería y Arquitectura, Universidad Central de Chile (UCEN), Santa Isabel 1186, Santiago 8370146, Chile.* luis.leyva@ucentral.cl

[f] *Núcleo de Investigación en Data Science (NIDS), Facultad de Ingeniería y Negocios, Universidad de Las Américas, Santiago 7500975, Chile.* oyanez@udla.cl

Computational Details

We systematically explored the potential energy surface using AUTOMATON,[1] which employs probabilistic cellular automata to generate initial structures and genetic algorithms to evolve them towards the global minimum. Calculations for singlet and triplet states were performed at the PBE0[2] -D3[3] /SDDAll[4-8] level. The lowest energy structures (Figure S1) were minimized at the PBE0-D3/def2-TZVP[9] level. For accurate energy comparisons, we conducted single-point energy calculations at the DLPNO-CCSD(T)[10-12]/CBS[13,14]//PBE0-D3/def2-TZVP level via Gaussian 16 software.[15] Chemical bonding was analyzed using the Adaptive Natural Density Partitioning[16-18] (AdNDP) technique via Multiwfn software.[19] Structure and AdNDP orbitals were visualized using CYLview 2.0[20] and VMD 1.9.3.[21]

The Interacting Quantum Atoms (IQA) method[22-25] was employed to decompose the interaction energy. The IQA analysis, which balances atomic deformation against additive interatomic interaction energies, was conducted at the PBE0-D3/def2-TZVP level using the AIMAll program.[26] The interaction energy, V_{IQA}^{int}, is the sum of the Coulombic, V_{C}^{int}, and exchange-correlation, V_{XC}^{int}, terms. V_{C}^{int} represents the exact electrostatic interaction between electrons and nuclei in a pair of basins, including nuclear repulsion, electron-nucleus attraction, and the Coulomb part of electron-electron repulsion. V_{XC}^{int} is purely quantum mechanical, depending on the exchange-correlation part of electron-electron interaction. Typically, V_{C}^{int} is associated with ionic-type interactions, while V_{XC}^{int} relates to covalent-type interactions.

The magnetically induced current density (J^{ind}) was calculated using the SYSMOIC program.[27] The external magnetic field was aligned parallel to the z-axis and perpendicular to the molecular plane using the CTOCD-DZ method to ensure origin-independent results. The Gaussian16 program was employed to obtain the perturbed molecular orbital with the CSGT keyword, which was then used to perform the actual calculation of density current.

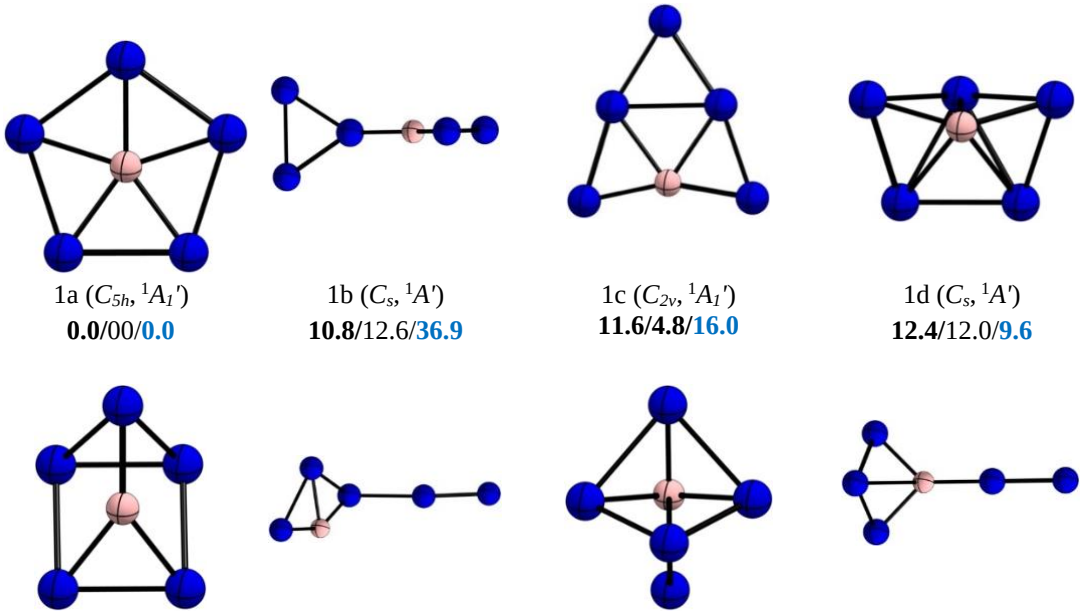

Figure S1. PBE0-D3/def2-TZVP geometries of the low-lying energy isomer of BSi_5^{3-}. Relative energies in kcal·mol^{-1} computed at DLPNO-CCSD(T)/CSB//PBE0-D3/def2-TZVP (**bold**), PBE0-D3/def2-TZVP including zero-point energy (ZPE) corrections and PBE0-PCM-D3/def2-TZVP (**blue**) levels. Point groups and spectroscopic states are also reported.

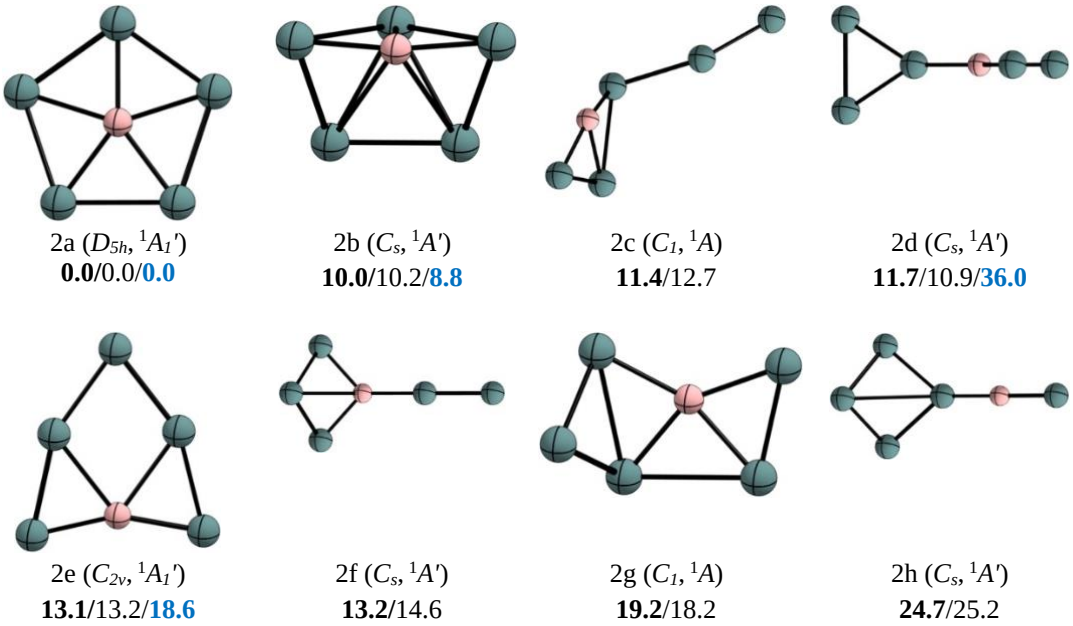

Figure S2. PBE0-D3/def2-TZVP geometries of the low-lying energy isomer of BGe_5^{3-} Relative energies in kcal·mol^{-1} computed at DLPNO-CCSD(T)/CSB//PBE0-D3/def2-TZVP (**bold**), PBE0-D3/def2-TZVP including zero-point energy (ZPE) corrections and PBE0-PCM-D3/def2-TZVP (**blue**) levels. Point groups and spectroscopic states are also reported.

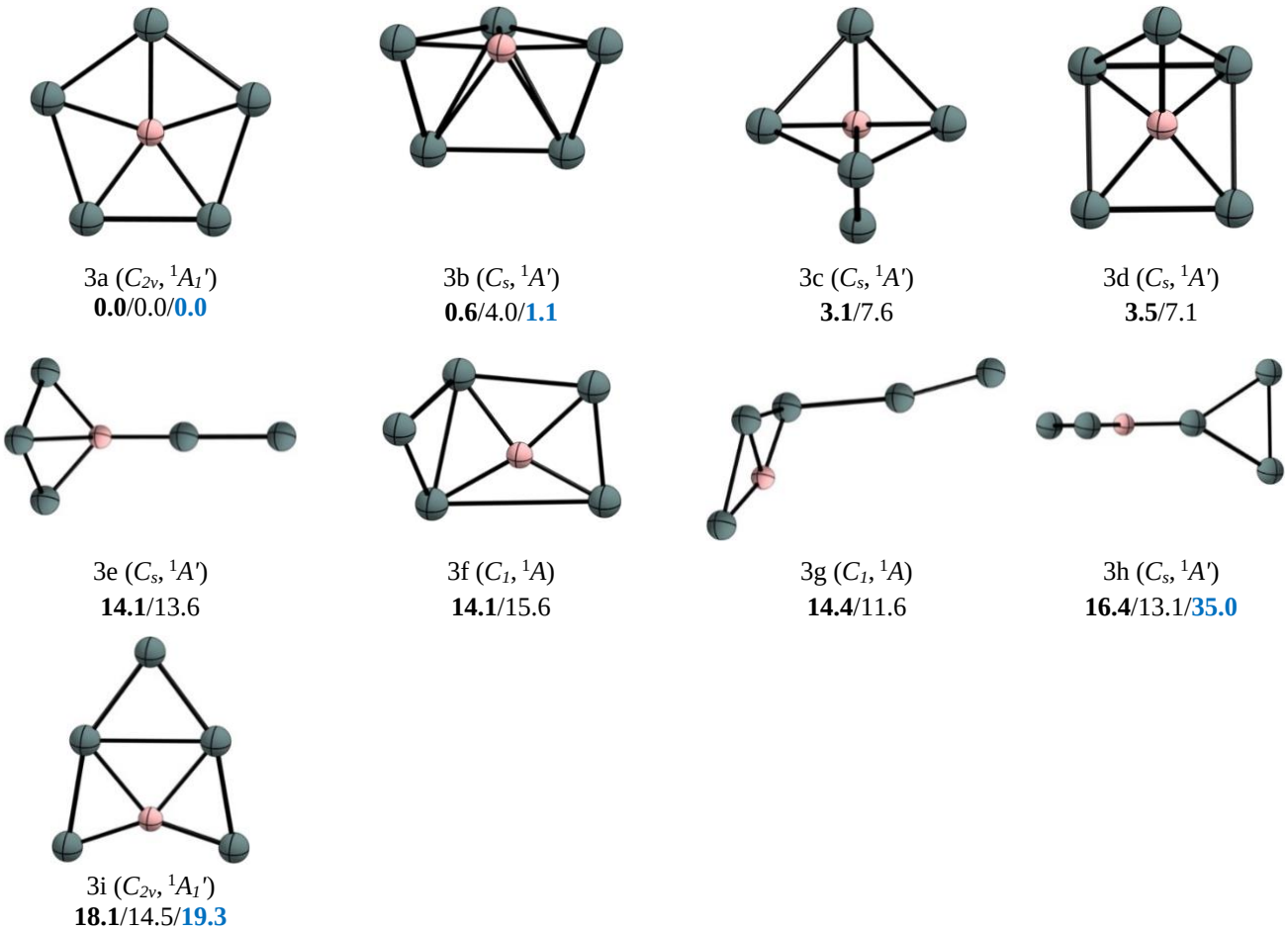

Figure S3. PBE0-D3/def2-TZVP geometries of the low-lying energy isomer of BSn_5^{3-} Relative energies in kcal·mol^{-1} computed at DLPNO-CCSD(T)/CSB//PBE0-D3/def2-TZVP (**bold**), PBE0-D3/def2-TZVP including zero-point energy (ZPE) corrections and PBE0-PCM-D3/def2-TZVP (**blue**) levels. Point groups and spectroscopic states are also reported.

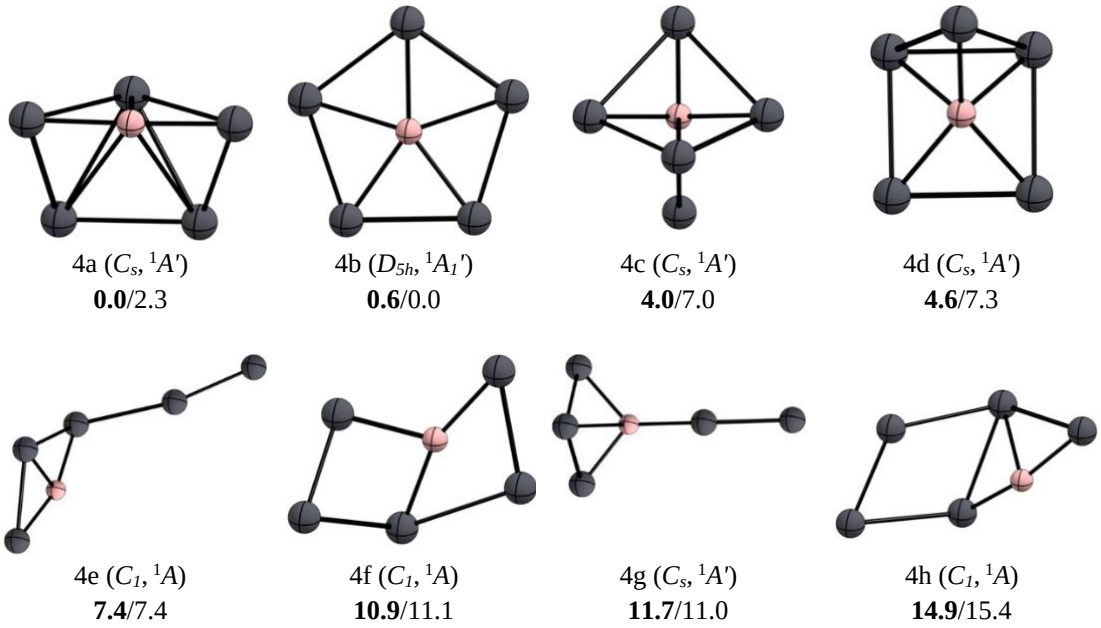

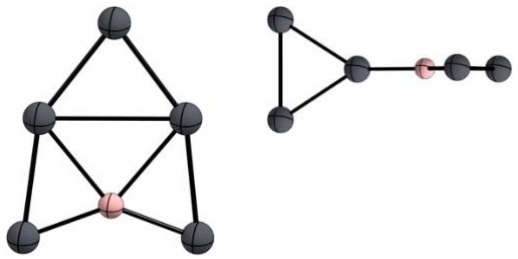

4i (C_{2v}, $^1A_1'$) **15.8**/13.2

4j (C_s, $^1A'$) **15.9**/14.1

Figure S4. PBE0-D3/def2-TZVP geometries of the low-lying energy isomer of CSi_5^{2-} Relative energies in kcal·mol^{-1} computed at DLPNO-CCSD(T)/CSB//PBE0-D3/def2-TZVP (**bold**) and PBE0-D3/def2-TZVP including zero-point energy (ZPE) corrections levels. Point groups and spectroscopic states are also reported.

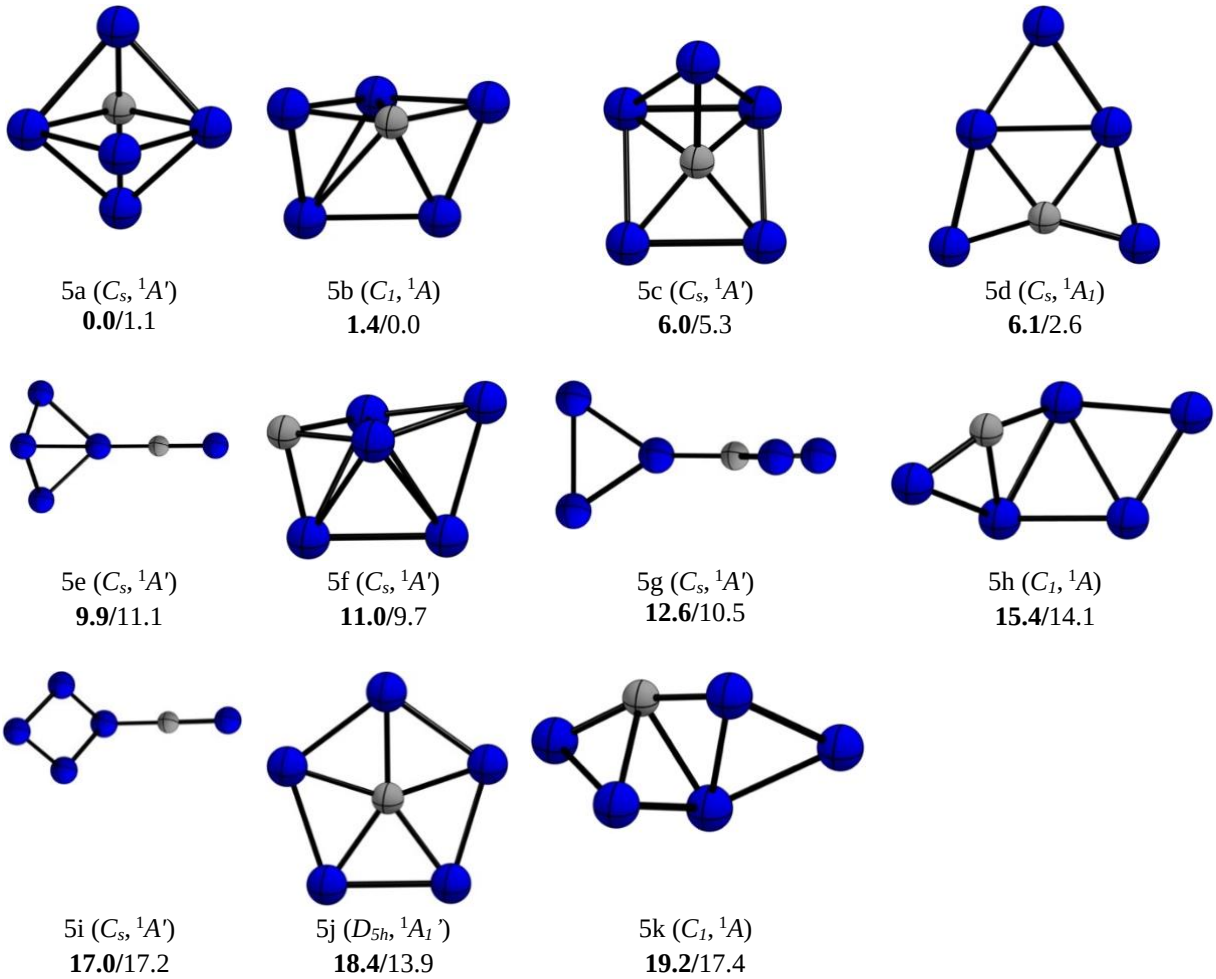

5a (C_s, $^1A'$) **0.0**/1.1

5b (C_1, ^1A) **1.4**/0.0

5c (C_s, $^1A'$) **6.0**/5.3

5d (C_s, $^1A_1$) **6.1**/2.6

5e (C_s, $^1A'$) **9.9**/11.1

5f (C_s, $^1A'$) **11.0**/9.7

5g (C_s, $^1A'$) **12.6**/10.5

5h (C_1, ^1A) **15.4**/14.1

5i (C_s, $^1A'$) **17.0**/17.2

5j (D_{5h}, $^1A_1'$) **18.4**/13.9

5k (C_1, ^1A) **19.2**/17.4

Figure S5. PBE0-D3/def2-TZVP geometries of the low-lying energy isomer of CSi_5^{2-} Relative energies in kcal·mol^{-1} computed at DLPNO-CCSD(T)/CSB//PBE0-D3/def2-TZVP (**bold**) and PBE0-D3/def2-TZVP including zero-point energy (ZPE) corrections levels. Point groups and spectroscopic states are also reported.

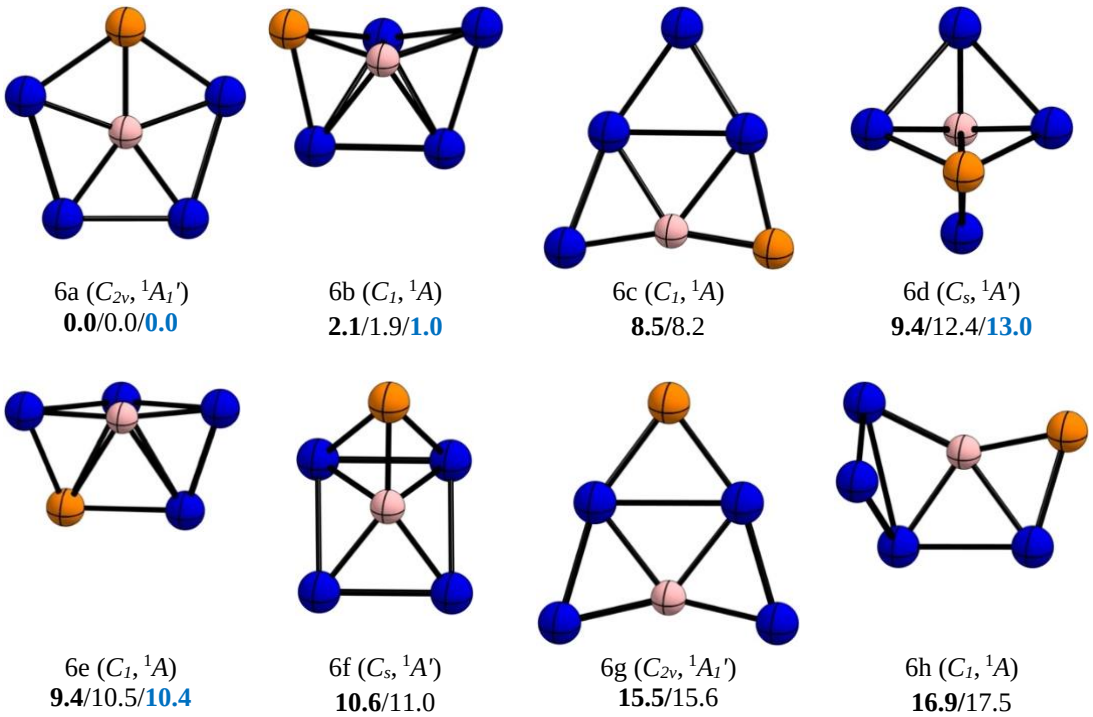

Figure S6. PBE0-D3/def2-TZVP geometries of the low-lying energy isomer of $BPSi_4^{2-}$ Relative energies in kcal·mol^{-1} computed at DLPNO-CCSD(T)/CSB//PBE0-D3/def2-TZVP (**bold**), PBE0-D3/def2-TZVP including zero-point energy (ZPE) corrections and PBE0-PCM-D3/def2-TZVP (**blue**) levels. Point groups and spectroscopic states are also reported.

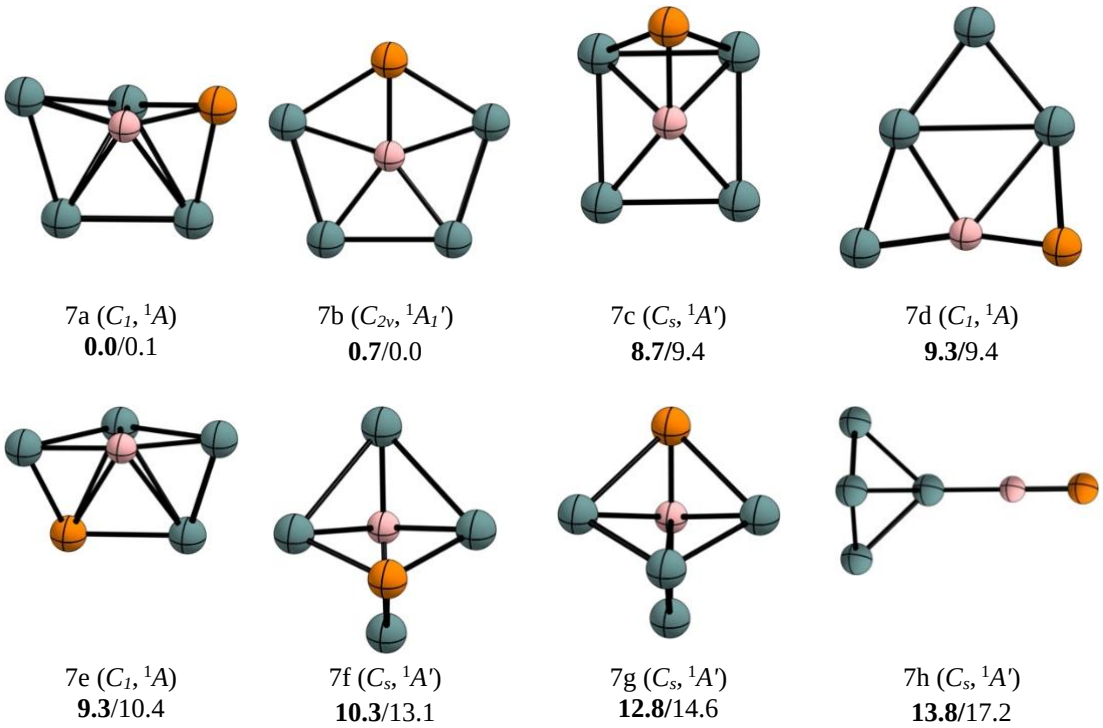

Figure S7. PBE0-D3/def2-TZVP geometries of the low-lying energy isomer of $BPGe_4^{2-}$ Relative energies in kcal·mol^{-1} computed at DLPNO-CCSD(T)/CSB//PBE0-D3/def2-TZVP (**bold**) and PBE0-D3/def2-TZVP including zero-point energy (ZPE) corrections and PBE0-PCM-D3/def2-TZVP (**blue**) levels. Point groups and spectroscopic states are also reported.

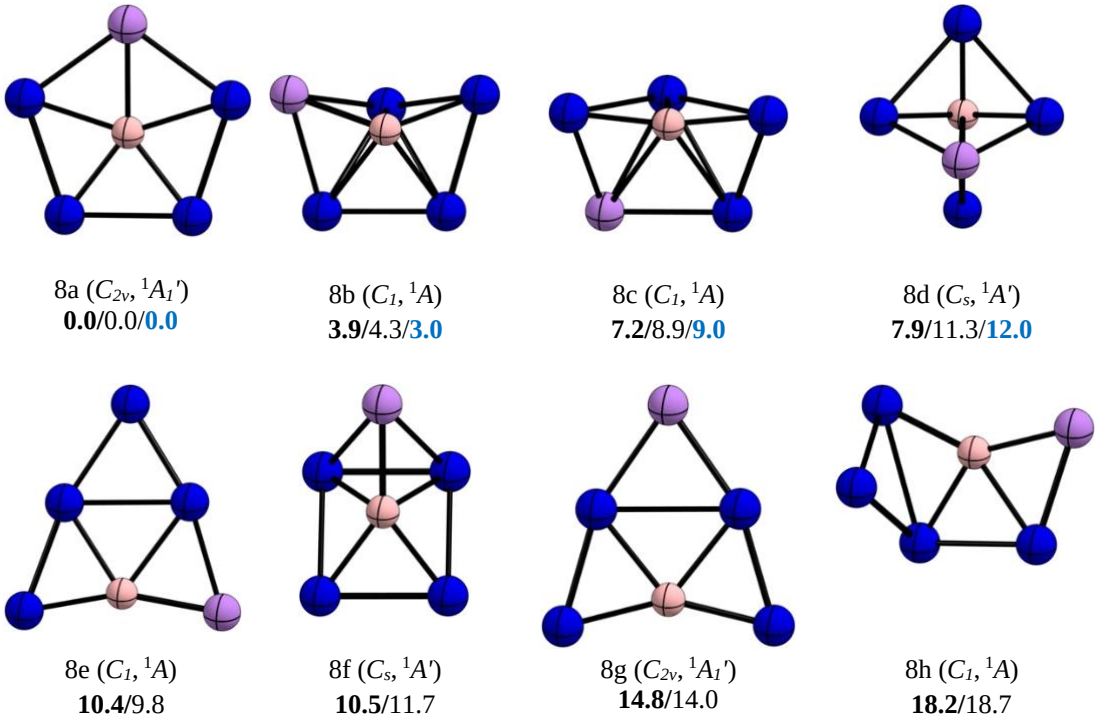

Figure S8. PBE0-D3/def2-TZVP geometries of the low-lying energy isomer of $BAsSi_4^{2-}$ Relative energies in kcal·mol^{-1} computed at DLPNO-CCSD(T)/CSB//PBE0-D3/def2-TZVP (**bold**), PBE0-D3/def2-TZVP including zero-point energy (ZPE) corrections and PBE0-PCM-D3/def2-TZVP (**blue**) levels. Point groups and spectroscopic states are also reported.

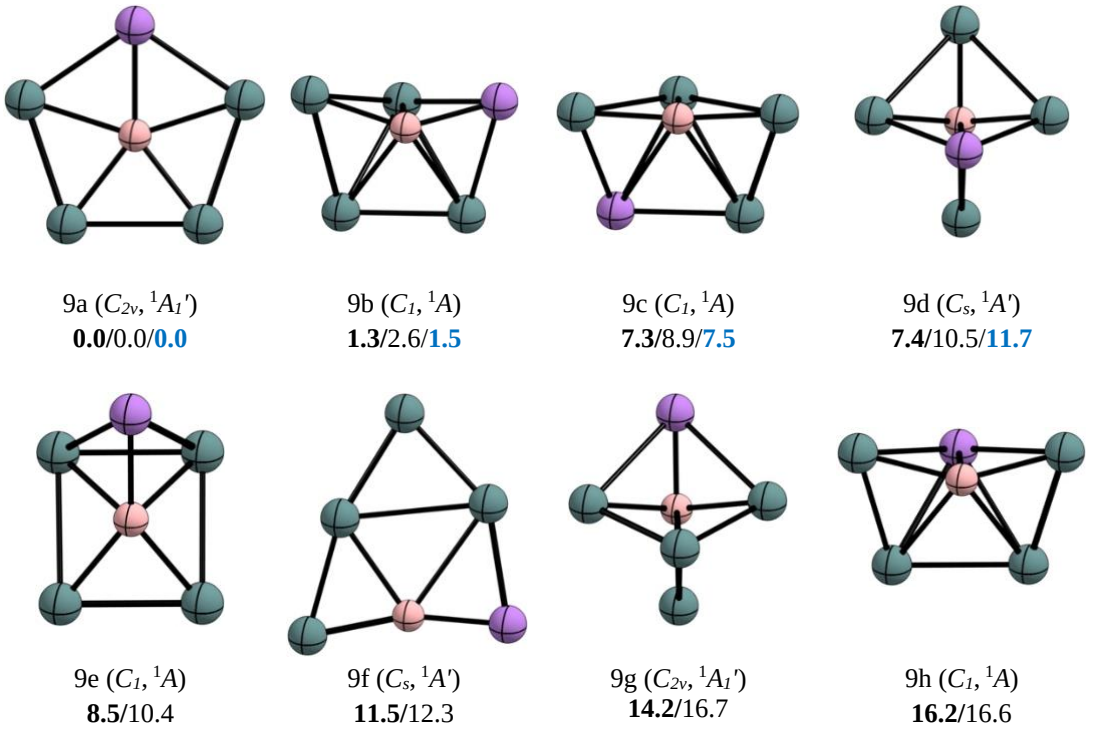

Figure S9. PBE0-D3/def2-TZVP geometries of the low-lying energy isomer of $BAsGe_4^{2-}$ Relative energies in kcal·mol^{-1} computed at DLPNO-CCSD(T)/CSB//PBE0-D3/def2-TZVP (**bold**), PBE0-D3/def2-TZVP including zero-point energy (ZPE) corrections and PBE0-PCM-D3/def2-TZVP (**blue**) levels. Point groups and spectroscopic states are also reported.

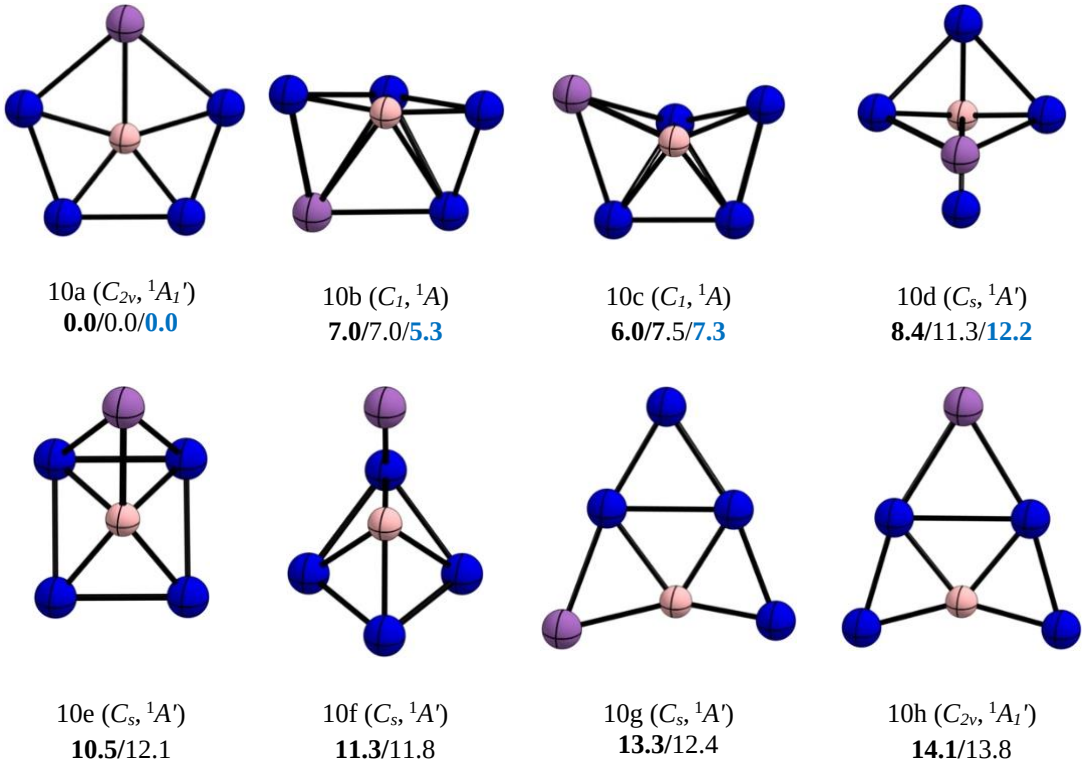

Figure S10. PBE0-D3/def2-TZVP geometries of the low-lying energy isomer of $BSbSi_4^{2-}$ Relative energies in kcal·mol^{-1} computed at DLPNO-CCSD(T)/CSB//PBE0-D3/def2-TZVP (**bold**), PBE0-D3/def2-TZVP including zero-point energy (ZPE) corrections and PBE0-PCM-D3/def2-TZVP (**blue**) levels. Point groups and spectroscopic states are also reported.

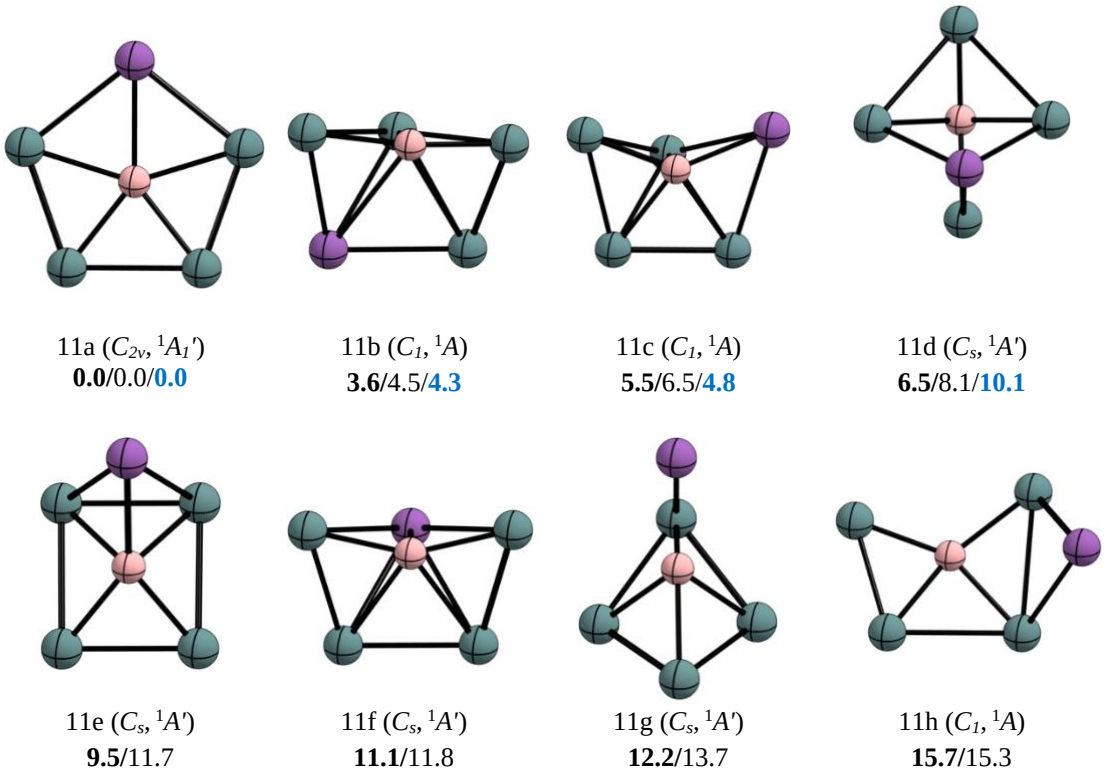

Figure S11. PBE0-D3/def2-TZVP geometries of the low-lying energy isomer of $BSbGe_4^{2-}$ Relative energies in kcal·mol^{-1} computed at DLPNO-CCSD(T)/CSB//PBE0-D3/def2-TZVP (**bold**), PBE0-D3/def2-TZVP including zero-point energy (ZPE) corrections and PBE0-PCM-D3/def2-TZVP (**blue**) levels. Point groups and spectroscopic states are also reported.

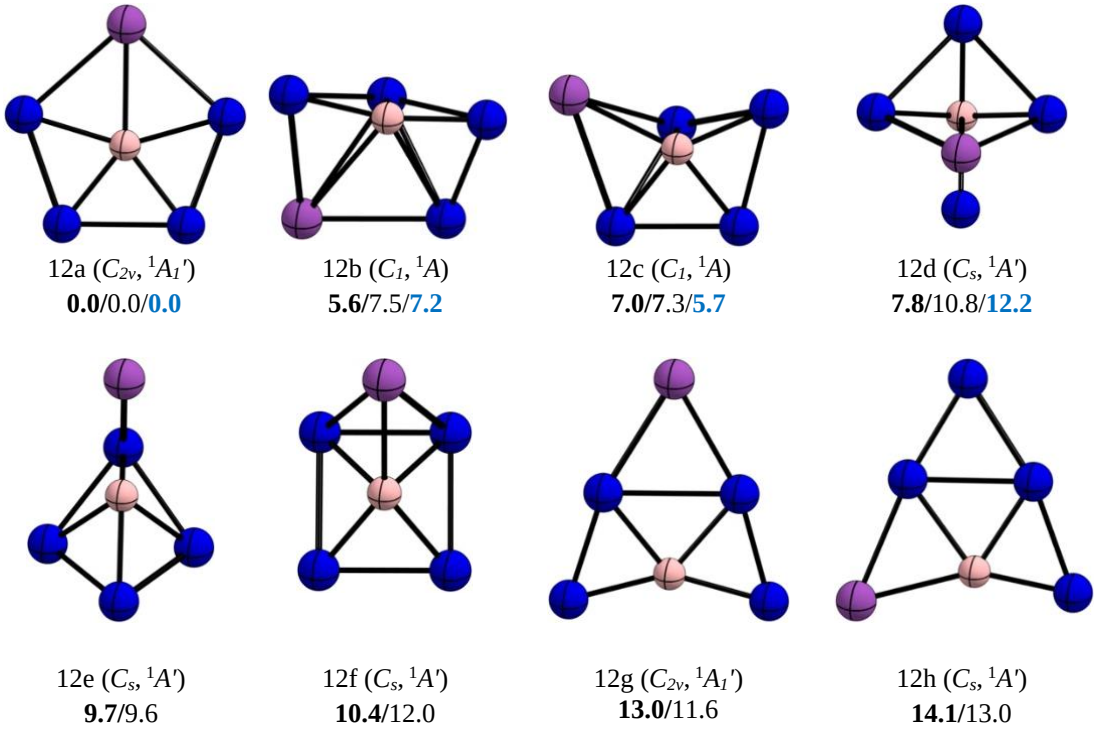

Figure S12. PBE0-D3/def2-TZVP geometries of the low-lying energy isomer of $BBiSi_4^{2-}$ .Relative energies in kcal·mol^{-1} computed at DLPNO-CCSD(T)/CSB//PBE0-D3/def2-TZVP (**bold**), PBE0-D3/def2-TZVP including zero-point energy (ZPE) corrections and PBE0-PCM-D3/def2-TZVP (**blue**) levels. Point groups and spectroscopic states are also reported.

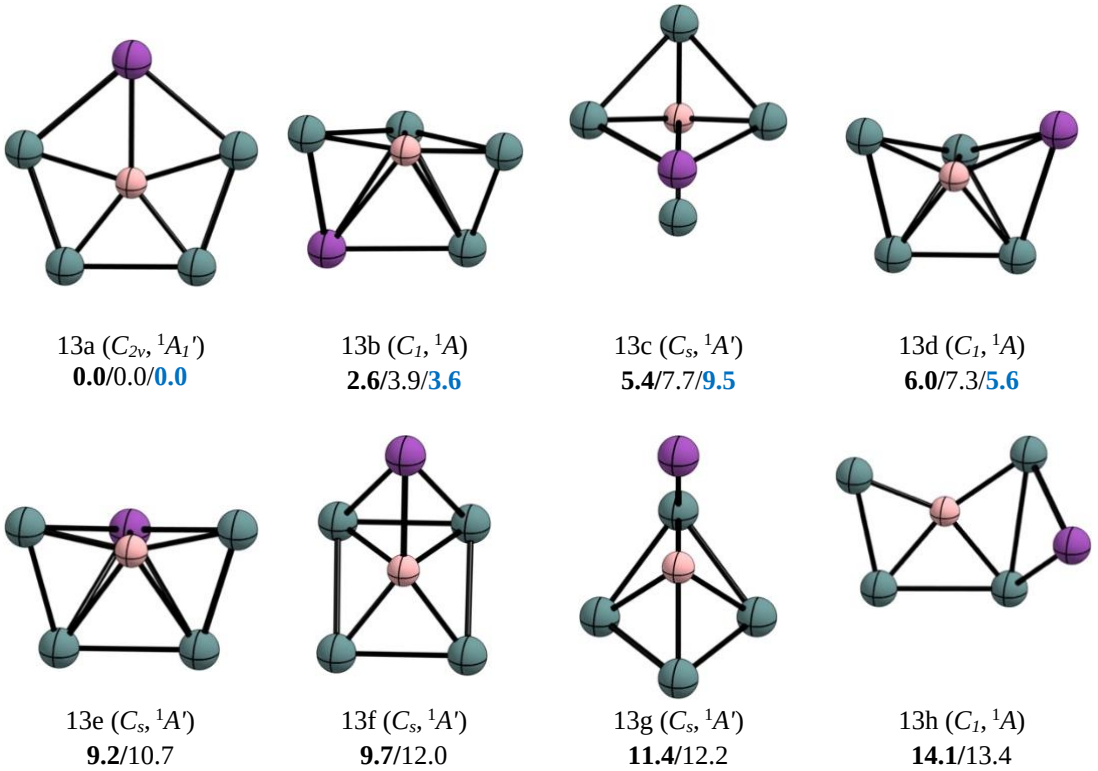

Figure S13. PBE0-D3/def2-TZVP geometries of the low-lying energy isomer of $BBiGe_4^{2-}$ Relative energies in kcal·mol^{-1} computed at DLPNO-CCSD(T)/CSB//PBE0-D3/def2-TZVP (**bold**), PBE0-D3/def2-TZVP including zero-point energy (ZPE) corrections and PBE0-PCM-D3/def2-TZVP (**blue**) levels. Point groups and spectroscopic states are also reported.

Table S1. Relative energies in kcal·mol^{-1} of $ETr_nPn_m^q$ (E=B-Tl, Tr = Si-Pb, Pn =P-Bi n=5-0, m=0-5 and q= –2, –1, 0, 1, 2) and their lowest harmonic vibrational frequency in cm^{-1} computed at the PBE0-D3/def2-TZVP level. Point groups also reported.

System	ΔE	ν_{min}	*Point group*	System	ΔE	ν_{min}	*Point group*	System	ΔE	ν_{min}	*Point group*
BSi_4P^{2-}	0.0	177.1	C_{2v}	BSn_2P_3	14.9	73.3	C_{2v}	BPb_2Bi_3	14.6	33.7	C_{2v}
$BSi_3P_2^-$	8.7	153.1	C_{2v}	$BSnP_4^+$	15.7	57.2	C_{2v}	$BPbBi_4^+$	18.0	31.6	C_{2v}
BSi_2P_3	7.7	105.3	C_{2v}	BSn_4As^{2-}	6.1	59.0	C_{2v}	BP_5^{2+}	4.8	193.6	C_{5v}
$BSiP_4^+$	9.4	92.3	C_s	$BSn_3As_2^-$	15.9	65.2	C_{2v}	BAs_5^{2+}	8.5	63.0	D_{5h}
BSi_4As^{2-}	0.0	154.1	C_{2v}	BSn_2As_3	14.3	58.8	C_{2v}	BSb_5^{2+}	15.4	51.8	D_{5h}
$BSi_3As_2^-$	5.9	146.2	C_{2v}	$BSnAs_4^+$	15.3	59.4	C_{2v}	BBi_5^{2+}	19.4	32.9	D_{5h}
BSi_2As_3	3.1	123.5	C_{2v}	BSn_4Sb^{2-}	2.3	55.3	C_{2v}	$AlSi_5^{3-}$	32.0	175.0	C_{5v}
$BSiAs_4^+$	6.2	105.0	C_{2v}	$BSn_3Sb_2^-$	11.2	52.3	C_{2v}	$AlGe_5^{3-}$	11.6	97.2	C_{5v}
BSi_4Sb^{2-}	0.0	136.3	C_{2v}	$BGeBi_4^+$	14.3	40.9	C_{2v}	$AlSn_5^{3-}$	5.5	59.0	C_{5v}
$BSi_3Sb_2^-$	1.6	118.2	C_{2v}	BSn_4P^{2-}	8.2	61.0	C_{2v}	$AlPb_5^{3-}$	1.2	36.9	C_{5v}
BSi_2Sb_3	5.2	80.1	C_{2v}	$BSn_3P_2^-$	9.4	9.2	C_{2v}	$GaSi_5^{3-}$	-	-	-
$BSiSb_4^+$	9.4	62.3	C_{2v}	BSn_2Sb_3	12.0	51.9	C_{2v}	$GaGe_5^{3-}$	16.7	94.0	C_{5v}
BSi_4Bi^{2-}	0.0	127.6	C_{2v}	$BSnSb_4^+$	14.5	48.3	C_{2v}	$GaSn_5^{3-}$	11.0	49.2	C_{5v}
$BSi_3Bi_2^-$	4.8	104.9	C_{2v}	BSn_4Bi^{2-}	1.0	51.0	C_{2v}	$GaPb_5^{3-}$	6.6	27.1	C_{5v}
BSi_2Bi_3	8.1	62.9	C_{2v}	$BSn_3Bi_2^-$	9.4	46.4	C_{2v}	$InSi_5^{3-}$	-	-	-
$BSiBi_4^+$	14.8	43.0	C_{2v}	BSn_2Bi_3	10.4	40.3	C_{2v}	$InGe_5^{3-}$	-	-	-
BGe_4P^{2-}	0.0	99.0	C_{2v}	$BSnBi_4^+$	15.7	37.6	C_{2v}	$InSn_5^{3-}$	27.7	58.6	C_{5v}
$BGe_3P_2^-$	10.5	120.8	C_{2v}	BPb_4P^{2-}	11.0	43.2	C_{2v}	$InPb_5^{3-}$	21.0	40.0	C_{5v}
BGe_2P_3	10.7	88.6	C_{2v}	$BPb_3P_2^-$	23.5	67.9	C_{2v}	$TlSi_5^{3-}$	-	-	-
$BGeP_4^+$	13.0	43.9	C_s	BPb_2P_3	16.5	65.9	C_{2v}	$TlGe_5^{3-}$	-	-	-
BGe_4As^{2-}	0.0	96.3	C_{2v}	$BPbP_4^+$	17.2	57.8	C_{2v}	$TlSn_5^{3-}$	-	-	-
$BGe_3As_2^-$	7.4	93.1	C_{2v}	BPb_4As^{2-}	9.2	41.9	C_{2v}	$TlPb_5^{3-}$	29.7	39.3	C_{5v}
BGe_2As_3	7.7	87.6	C_{2v}	$BPb_3As_2^-$	20.3	51.0	C_{2v}				
$BGeAs_4^+$	10.5	81.1	C_{2v}	BPb_2As_3	17.0	47.7	C_{2v}				
BGe_4Sb^{2-}	0.0	85.7	C_{2v}	$BPbAs_4^+$	17.8	50.4	C_{2v}				
$BGe_3Sb_2^-$	1.5	75.2	C_{2v}	BPb_4Sb^{2-}	5.6	39.1	C_{2v}				
BGe_2Sb_3	5.7	67.8	C_{2v}	$BPb_3Sb_2^-$	14.7	41.4	C_{2v}				
$BGeSb_4^+$	10.9	59.7	C_{2v}	BPb_2Sb_3	15.6	41.1	C_{2v}				
BGe_4Bi^{2-}	0.0	78.1	C_{2v}	$BPbSb_4^+$	17.6	41.0	C_{5v}				
$BGe_3Bi_2^-$	1.6	63.1	C_{2v}	BPb_4Bi^{2-}	3.6	37.9	C_{2v}				
BGe_2Bi_3	7.0	50.7	C_{2v}	$BPb_3Bi_2^-$	12.7	35.1	C_{2v}				

Table S2. Singlet-triplet energy gap in kcal·mol^{-1}, smallest vibrational frequencies in cm^{-1} and T_1 diagnostics for the global minimum of BTr_5^{3-} (Tr = Si-Sn) and BTr_4Pn^{2-} (Tr = Si for Pn = P-Bi and Tr = Ge for Pn = As-Bi).

System	ΔE_{S-T}	ν_{min}	*T_1 Diagnostic*
BSi_5^{3-}	32.6	177.1	0.019
BGe_5^{3-}	29.5	98.4	0.012
BSn_5^{3-}	20.8	56.4	0.016
BSi_4P^{2-}	22.1	177.1	0.021
BSi_4As^{2-}	30.4	154.1	0.018
BGe_4As^{2-}	25.7	98.3	0.013
BSi_4Sb^{2-}	22.4	136.3	0.019
BGe_4Sb^{2-}	22.5	85.7	0.013
BSi_4Bi^{2-}	20.5	127.6	0.020
BGe_4Bi^{2-}	20.7	78.1	0.013

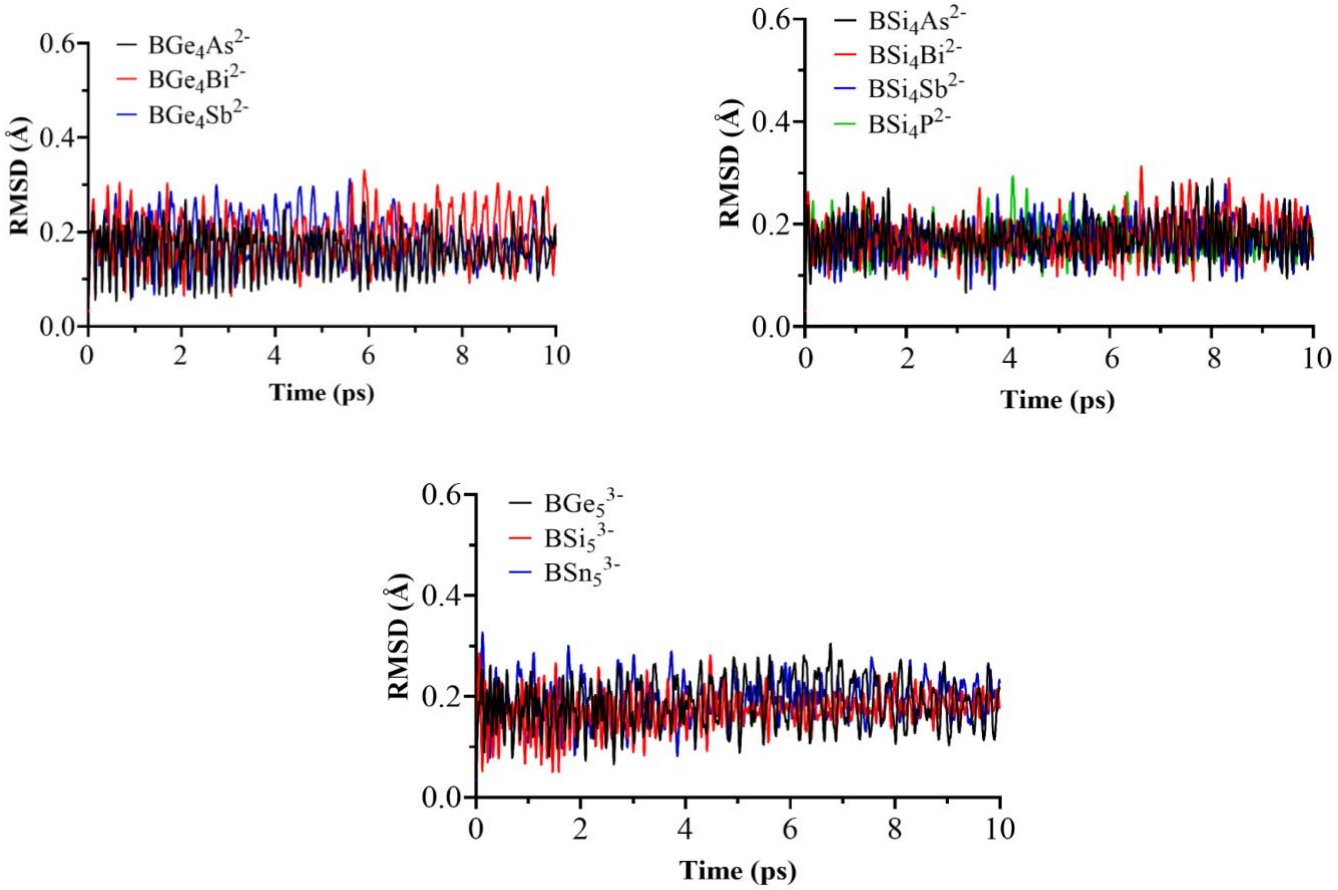

Figure S14. RMSD curves along the trajectories of Born-Oppenheimer molecular dynamics simulations for all global minima of ppB.

Table S3. Bond lengths (r, Å), natural charges (q, |e|) and Wiberg bond indices (WBI) of BTr_5^{3-} (Tr = Si-Sn) and BTr_4Pn^{2-} (Pn = P-Bi for Tr = Si and Pn = As-Bi for Tr = Ge), at the PBE0-D3/def2-TZVP level

System	r_{Tr-Tr}	r_{Tr-B}	r_{Tr-Pn}	r_{Pn-B}	q(Tr)	q(B)	q(Pn)	WBI_{Tr-Tr}	WBI_{Tr-B}	WBI_{Tr-Pn}	WBI_{Pn-B}
BSi_5^{3-}	2.40	2.04	-	-	−0.36	−1.18	-	0.81	0.81	-	-
BGe_5^{3-}	2.52	2.15	-	-	−0.40	−1.00	-	0.80	0.82	-	-
BSn_5^{3-}	2.85	2.42	-	-	−0.38	−1.09	-	0.79	0.80	-	-
BSi_4P^{2-}	2.35-2.43	1.99-2.04	2.31	1.92	−0.05-0.16	−1.16	−0.39	0.68-0.89	0.66-0.89	0.70	0.93
BSi_4As^{2-}	2.33-2.43	1.99-2.06	2.42	2.05	−0.10-0.15	−1.17	−0.32	0.64-0.93	0.69-0.91	0.70	0.86
BGe_4As^{2-}	2.46-2.55	2.10-2.16	2.49	2.07	−0.10-0.15	−1.01	−0.36	0.64-0.90	0.68-0.90	0.68	0.91
BSi_4Sb^{2-}	2.3-2.45	1.99-2.09	2.62	2.29	−0.1-0.18	−1.18	−0.21	0.57-0.98	0.74-0.93	0.71	0.69
BGe_4Sb^{2-}	2.44-2.57	2.09-2.19	2.67	2.31	−0.14-0.19	−1.07	−0.24	0.56-0.95	0.73-0.94	0.71	0.72
BSi_4Bi^{2-}	2.30-2.46	1.99-2.10	2.70	2.39	−0.1-0.20	−1.15	−0.22	0.55-1.02	0.76-0.94	0.70	0.64
BGe_4Bi^{2-}	2.43-2.59	2.09-2.20	2.75	2.42	−0.14-0.21	−1.04	−0.24	0.54-0.99	0.75-0.95	0.70	0.67

	Tr-LPs Pn-LPs	Tr-B-Tr σ-bonds Tr-B-Pn σ-bonds	B-Tr_4Pn π bonds
	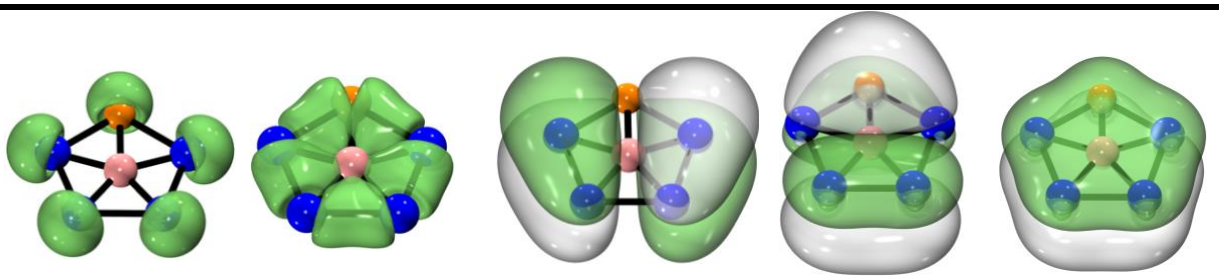		
	5 x 1c-2e	5 x 3c-2e	3x 6c-2e
B, Tr=Si, Pn=P	ON = 1.84-1.89 |e|	ON = 1.99 |e|	ON = 2.00 |e|
B,Tr=Si,Pn=As	ON = 1.8-1.91 |e|	ON = 1.99 |e|	ON = 2.00 |e|
B,Tr=Si,Pn=Sb	ON = 1.83-1.93 |e|	ON = 1.99 |e|	ON = 2.00 |e|
B,Tr=Si, Pn=Bi	ON = 1.82-1.94 |e|	ON = 1.99 |e|	ON = 2.00 |e|
B,Tr=Ge,Pn=As	ON = 1.87-1.91 |e|	ON = 1.99 |e|	ON = 2.00 |e|
B,Tr=Ge,Pn=Sb	ON = 1.86-1.93 |e|	ON = 1.99 |e|	ON = 2.00 |e|
B,Tr=Ge,Pn=Bi	ON = 1.86-1.94 |e|	ON = 1.99 |e|	ON = 2.00 |e|

Figure S15. Adaptive Natural Density Partitioning bonding pattern for BTr_4Pn^{2-} (Pn = P-Bi for Tr = Si and Pn = As-Bi for Tr = Ge) at the PBE0-D3/def2-TZVP level.

Table S4. Energy components of IQA and delocalization indices (δ) between atom pairs for BTr_4Pn^{2-} (Pn = P-Bi for Tr = Si and Pn = As-Bi for Tr = Ge). ΔE_{IQA} is the total integration error in IQA energies, V_{IQA}^{int}, V_{C}^{int}, and V_{XC}^{int} are interatomic IQA interaction energy, Coulomb energy component, and exchange-correlation energy component of the interaction energy, respectively, in kcal·mol^{-1}.

	BSi_4P^{2-}	BSi_4As^{2-}	BSi_4Sb^{2-}	BSi_4Bi^{2-}	BGe_4As^{2-}	BGe_4Sb^{2-}	BGe_4Bi^{2-}
ΔE_{IQA}	0.0	0.0	0.0	0.0	0.0	0.0	0.0
V_{IQA}^{int}(B-Tr)	–410.9/–505.1	–393.0/–509.6	–338.8/–509.7	–319.3/–496.2	–114.9/–139.0	–112.4/–145.3	–109.8/–144.8
V_{C}^{int}(B-Tr)	–305.6/–357.9	–280.9/–362.4	–219.5/–364.5	–199.8/–351.5	–22.6/–20.3	–14.2/–23.5	–11.1/–22.7
V_{XC}^{int}(B-Tr)	–105.3/–147.2	–112.1/–147.2	–119.3/–145.2	–119.5/–144.7	–92.3/–118.7	–98.2/–121.8	–98.7/–122.1
V_{IQA}^{int}(B-Pn)	66.6	–4.3	–110.9	–90.5	–94.6	–101.9	–85.5
V_{C}^{int}(B-Pn)	252.5	157.7	12.9	18.8	41.7	3.6	7.7
V_{XC}^{int}(B-Pn)	–185.9	–162.0	–123.8	–109.3	–136.3	–105.5	–93.1
V_{IQA}^{int}(Tr-Tr)	22.5/26.4	10.6/28.3	–10.9/33.8	–17.9/33.1	–81.9/–58.6	–85.8/–53.5	–88.3/–51.5
V_{C}^{int}(Tr-Tr)	95.1/84.9	87.7/84.5	74.8/85.0	71.8/82.6	19.4/18.4	19.5/17.3	19.8/16.8
V_{XC}^{int}(Tr-Tr)	–72.5/–58.4	–77.1/-56.2	–85.7/–51.2	–89.7/–49.6	–101.3/–77.1	–105.2/–70.8	–108.1/–68.3
V_{IQA}^{int}(Tr-Pn)	–194.3	–123.6	–67.5	–66.0	–90.3	–72.8	–69.8
V_{C}^{int}(Tr-Pn)	–101.1	–35.1	17.4	15.0	5.3	16.8	15.2
V_{XC}^{int}(Tr-Pn)	–93.2	–88.4	–84.9	–81.0	–95.6	–89.6	–85.0
δ(B-Tr)	0.8/1.1	0.9/1.1	0.9/1.1	0.9/1.1	0.7/0.9	0.8/1.0	0.8/1.0
δ(B-Pn)	1.3	1.2	1.0	0.9	1.0	0.8	0.8
δ(Tr-Tr)	0.7/0.6	0.8/0.5	0.8/0.5	0.8/0.5	1.0/0.7	1.0/0.7	1.0/0.6
δ(Tr-Pn)	0.8	0.8	0.8	0.8	0.9	0.9	0.9

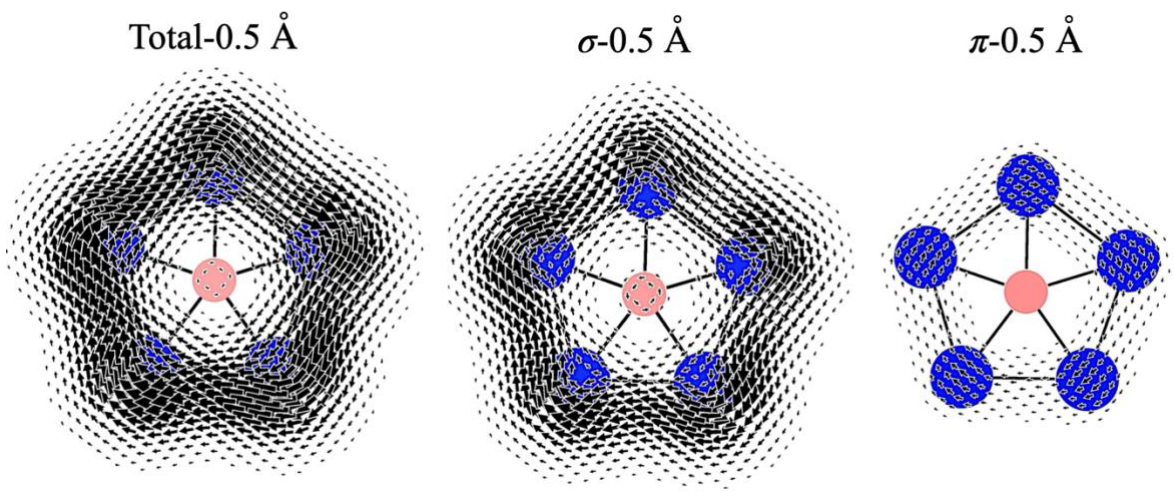

System	BSi_5^{3-}	BGe_5^{3-}	BSn_5^{3-}	BSi_4P^{2-}	BSi_4As^{2-}	BSi_4Sb^{2-}	BSi_4Bi^{2-}	BGe_4As^{2-}	BGe_4Sb^{2-}	BGe_4Bi^{2-}
Total	32.5	37.5	38.7	31.5	31.6	32.7	32.8	35.7	36.1	35.9
σ	21.0	25.5	26.9	21.3	22.3	23.5	23.9	25.1	26.3	26.7
π	11.5	11.9	11.9	10.4	10.1	8.9	8.2	10.7	9.5	8.7

Figure S16. Vector plots in the molecular plane 0.5 Å above the molecular plane for BTr_4Pn^{2-} (Pn = P-Bi for Tr = Si and Pn = As-Bi for Tr = Ge) system and RCSs (total, σ and π, in nA/T) for each system at the PBE0-D3/def2-TZVP level.

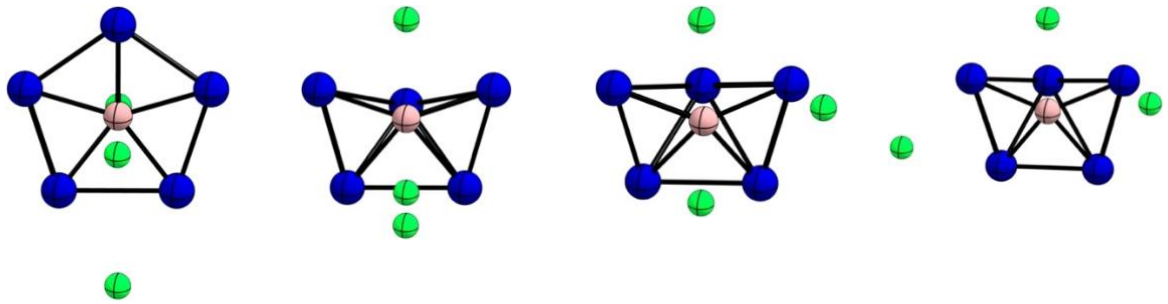

24a **0.0**/0.0 | 24b **0.6**/1.9 | 24c **0.8**/0.1 | 24d **2.3**/2.6

Figure S17. Global minimum and low-lying isomers of cluster BLi_3Si_5. Relative energies are shown in kcal·mol^{-1} at DLPNO-CCSD(T)/CSB//PBE0-D3/def2-TZVP (**in bold**) and PBE0-D3/def2-TZVP levels, including zero-point energy (ZPE) corrections.

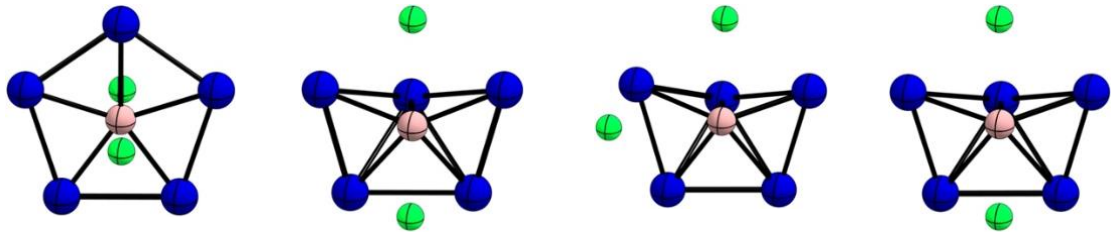

25a **0.0**/0.0 | 25b **2.5**/2.7 | 25c **5.6**/5.8 | 25d **7.3**/8.6

Figure S18. Global minimum and low-lying isomers of cluster $BLi_2Si_5^-$. Relative energies are shown in kcal·mol^{-1} at DLPNO-CCSD(T)/CSB//PBE0-D3/def2-TZVP (**in bold**) and PBE0-D3/def2-TZVP levels, including zero-point energy (ZPE) corrections.

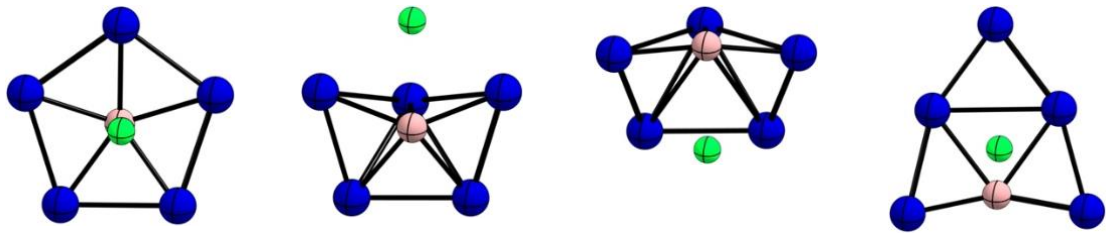

26a **0.0**/0.0 | 26b **4.3**/5.8 | 26c **14.3**/17.8 | 26d **18.1**/17.0

Figure S19. Global minimum and low-lying isomers of cluster $BLiSi_5^{2-}$. Relative energies are shown in kcal·mol^{-1} at DLPNO-CCSD(T)/CSB//PBE0-D3/def2-TZVP (**in bold**) and PBE0-D3/def2-TZVP levels, including zero-point energy (ZPE) corrections.

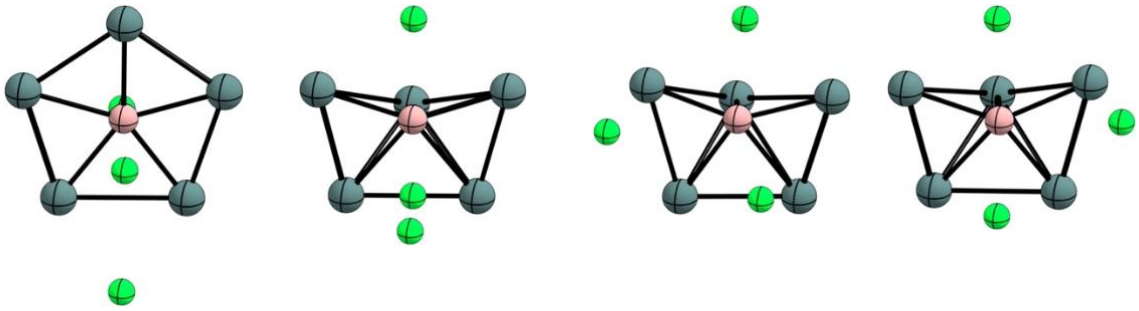

27a
0.0/0.0

27b
1.4/2.1

27c
2.9/3.4

27d
3.0/2.0

Figure S20. Global minimum and low-lying isomers of cluster BLi_3Ge_5. Relative energies are shown in kcal·mol^{-1} at DLPNO-CCSD(T)/CSB//PBE0-D3/def2-TZVP (**in bold**) and PBE0-D3/def2-TZVP levels, including zero-point energy (ZPE) corrections.

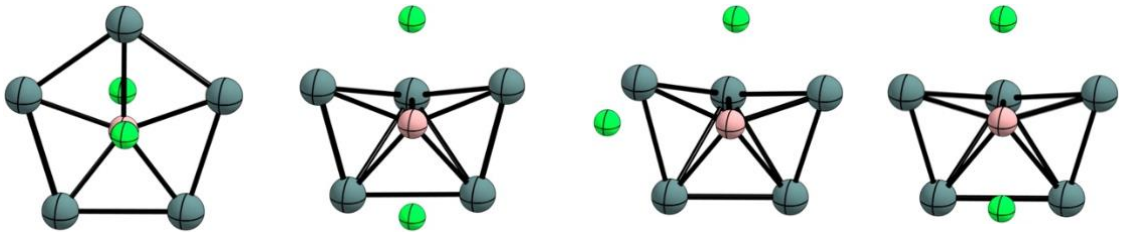

28a
0.0/0.0

28b
3.4/6.0

28c
8.1/7.4

28d
8.1/8.5

Figure S21. Global minimum and low-lying isomers of cluster $BLi_2Ge_5^-$. Relative energies are shown in kcal·mol^{-1} at DLPNO-CCSD(T)/CSB//PBE0-D3/def2-TZVP (**in bold**) and PBE0-D3/def2-TZVP levels, including zero-point energy (ZPE) corrections.

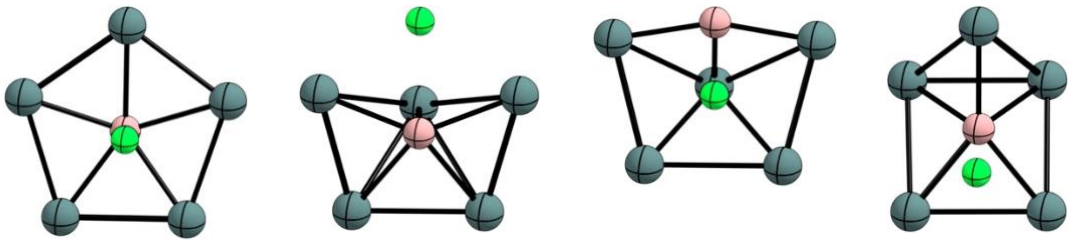

29a
0.0/0.0

29b
4.9/5.5

29b
10.1/11.3

29d
15.0/15.8

Figure S22. Global minimum and low-lying isomers of cluster $BLiGe_5^{2-}$. Relative energies are shown in kcal·mol^{-1} at DLPNO-CCSD(T)/CSB//PBE0-D3/def2-TZVP (**in bold**) and PBE0-D3/def2-TZVP levels, including zero-point energy (ZPE) corrections.

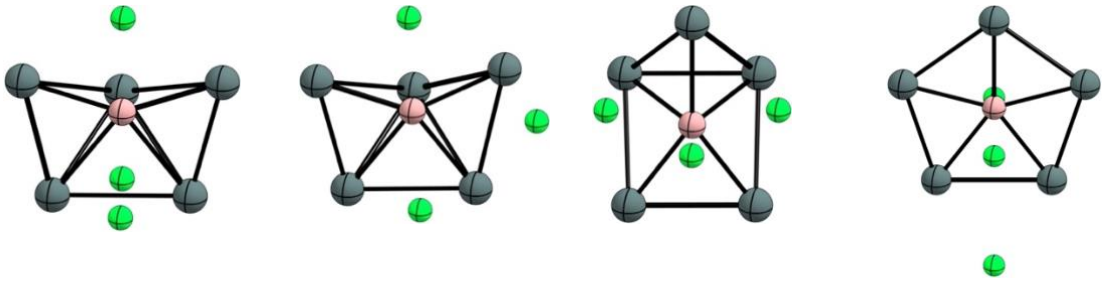

30a **0.0**/0.0 | 30b **4.7**/4.1 | 30b **5.6**/5.8 | 30d **7.0**/4.1

Figure S23. Global minimum and low-lying isomers of cluster BLi_3Sn_5. Relative energies are shown in kcal·mol^{-1} at DLPNO-CCSD(T)/CSB//PBE0-D3/def2-TZVP (**in bold**) and PBE0-D3/def2-TZVP levels, including zero-point energy (ZPE) corrections.

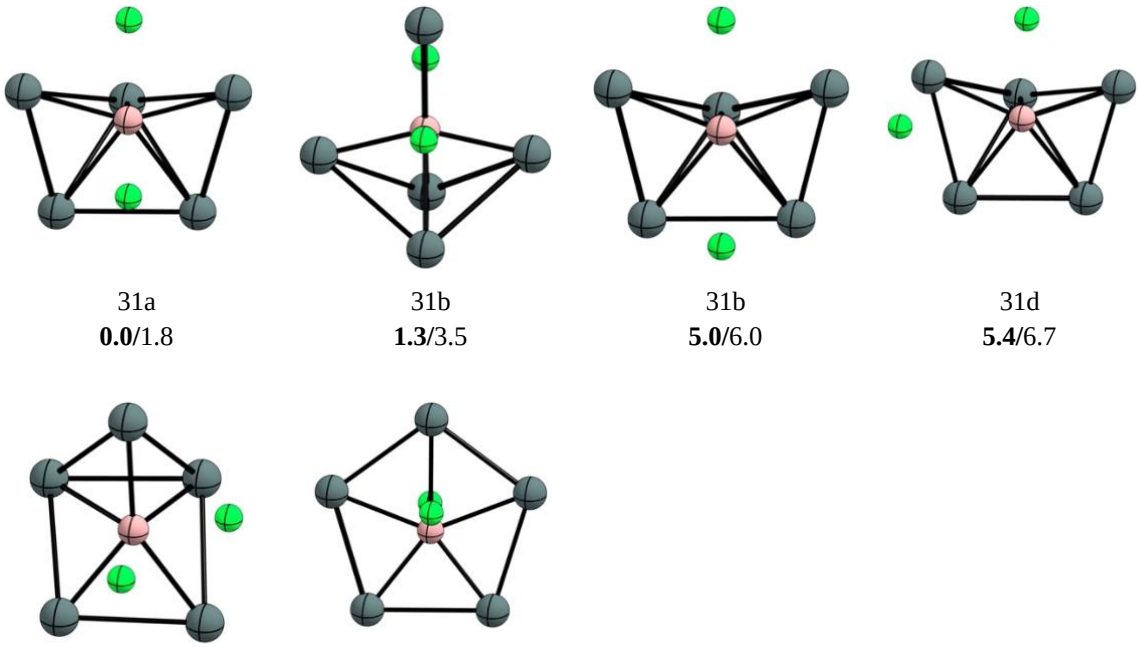

31a **0.0**/1.8 | 31b **1.3**/3.5 | 31b **5.0**/6.0 | 31d **5.4**/6.7

31e **6.7**/6.8 | 31g **7.2**/0.0

Figure S24. Global minimum and low-lying isomers of cluster $BLi_2Sn_5^-$. Relative energies are shown in kcal·mol^{-1} at DLPNO-CCSD(T)/CSB//PBE0-D3/def2-TZVP (**in bold**) and PBE0-D3/def2-TZVP levels, including zero-point energy (ZPE) corrections.

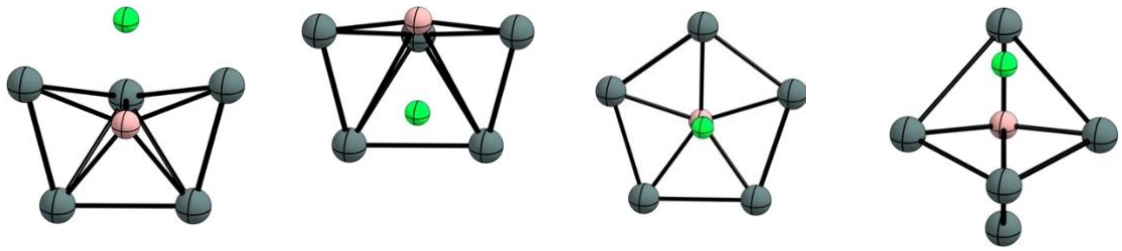

32a **0.0**/1.1 | 32b **2.0**/1.0 | 32b **2.4**/0.0 | 32d **6.8**/6.1

Figure S25. Global minimum and low-lying isomers of cluster $BLiSn_5^{2-}$. Relative energies are shown in kcal·mol^{-1} at DLPNO-CCSD(T)/CSB//PBE0-D3/def2-TZVP (**in bold**) and PBE0-D3/def2-TZVP levels, including zero-point energy (ZPE) corrections.

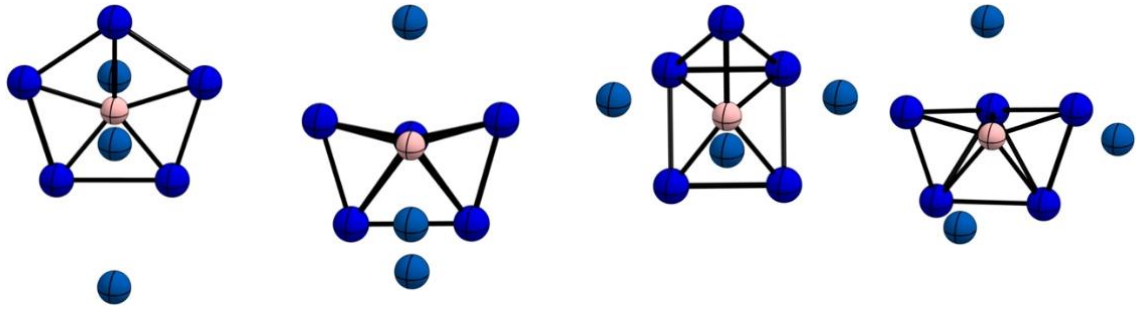

33a **0.0**/0.0 | 33b **6.3**/4.5 | 33c **7.3**/6.7 | 33d **8.7**/6.1

Figure S26. Global minimum and low-lying isomers of cluster BNa_3Si_5. Relative energies are shown in kcal·mol^{-1} at DLPNO-CCSD(T)/CSB//PBE0-D3/def2-TZVP (**in bold**) and PBE0-D3/def2-TZVP levels, including zero-point energy (ZPE) corrections.

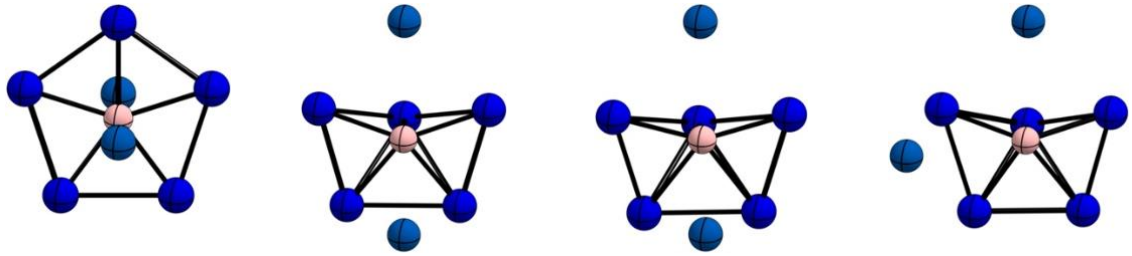

34a **0.0**/0.0 | 34b **12.6**/9.5 | 34c **15.5**/13.8 | 34d **16.5**/13.2

Figure S27. Global minimum and low-lying isomers of cluster $BNa_2Si_5^{-}$. Relative energies are shown in kcal·mol^{-1} at DLPNO-CCSD(T)/CSB//PBE0-D3/def2-TZVP (**in bold**) and PBE0-D3/def2-TZVP levels, including zero-point energy (ZPE) corrections.

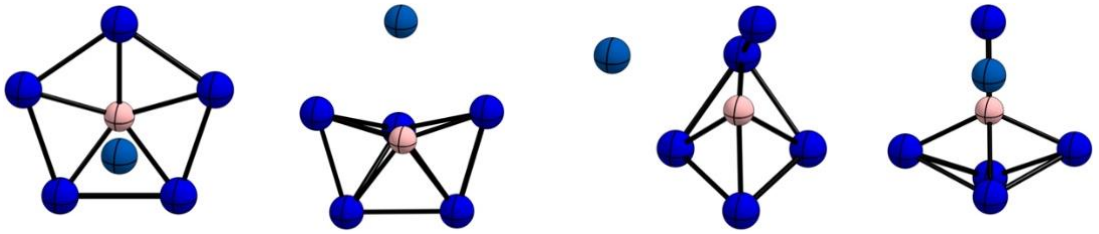

35a **0.0**/0.0 | 35b **10.8**/9.7 | 35c **11.5**/8.3 | 35d **13.0**/12.0

Figure S28. Global minimum and low-lying isomers of cluster $BNaSi_5^{2-}$. Relative energies are shown in kcal·mol^{-1} at DLPNO-CCSD(T)/CSB//PBE0-D3/def2-TZVP (**in bold**) and PBE0-D3/def2-TZVP levels, including zero-point energy (ZPE) corrections.

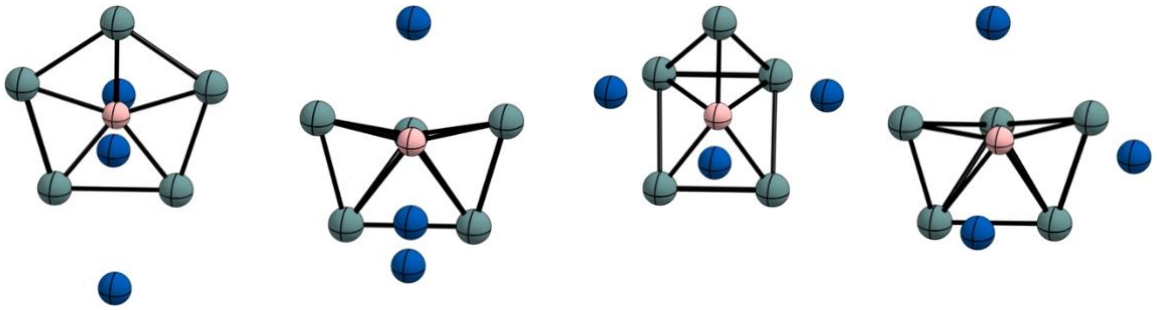

36a **0.0**/0.0 | 36b **4.9**/4.6 | 36c **6.2**/7.4 | 36d **6.3**/5.8

Figure S29. Global minimum and low-lying isomers of cluster BNa_3Ge_5. Relative energies are shown in kcal·mol^{-1} at DLPNO-CCSD(T)/CSB//PBE0-D3/def2-TZVP (**in bold**) and PBE0-D3/def2-TZVP levels, including zero-point energy (ZPE) corrections.

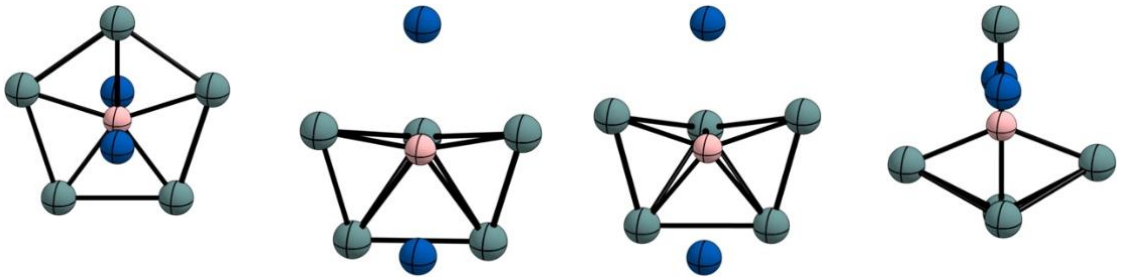

37a **0.0**/0.0 | 37b **14.4**/13.0 | 37c **12.5**/12.3 | 37d **15.5**/13.3

Figure S30. Global minimum and low-lying isomers of cluster $BNa_2Ge_5^{-}$. Relative energies are shown in kcal·mol^{-1} at DLPNO-CCSD(T)/CSB//PBE0-D3/def2-TZVP (**in bold**) and PBE0-D3/def2-TZVP levels, including zero-point energy (ZPE) corrections.

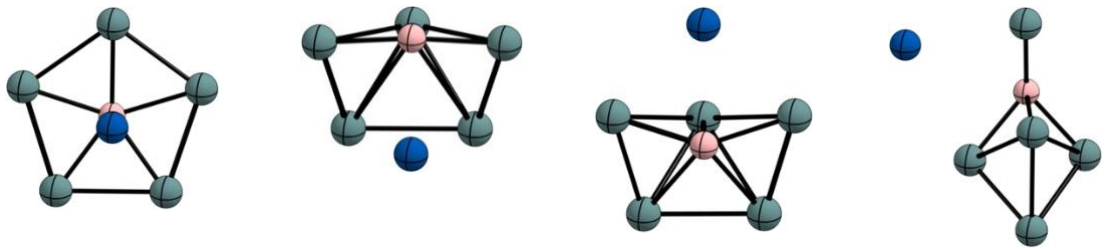

38a
0.0/0.0

38b
4.9/5.5

38b
10.1/11.3

38d
15.0/15.8

Figure S31. Global minimum and low-lying isomers of cluster $BNaGe_5^{2-}$. Relative energies are shown in kcal·mol^{-1} at DLPNO-CCSD(T)/CSB//PBE0-D3/def2-TZVP (**in bold**) and PBE0-D3/def2-TZVP levels, including zero-point energy (ZPE) corrections.

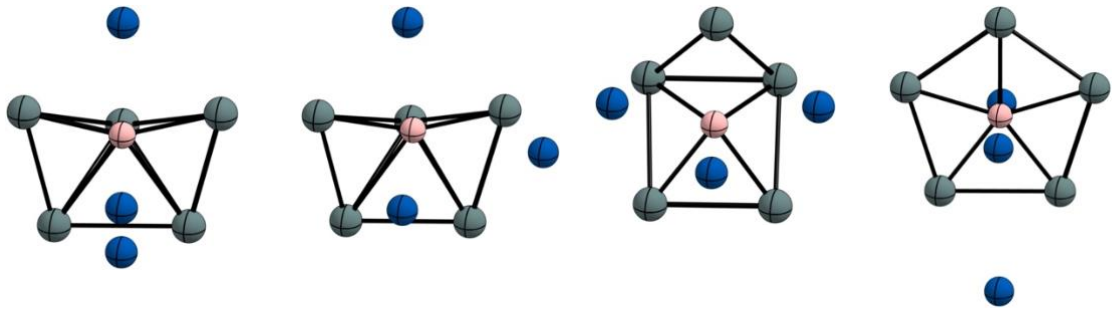

39a
0.0/0.0

39b
0.4/0.2

39b
1.8/4.0

39d
4.2/1.2

Figure S32. Global minimum and low-lying isomers of cluster BNa_3Sn_5. Relative energies are shown in kcal·mol^{-1} at DLPNO-CCSD(T)/CSB//PBE0-D3/def2-TZVP (**in bold**) and PBE0-D3/def2-TZVP levels, including zero-point energy (ZPE) corrections.

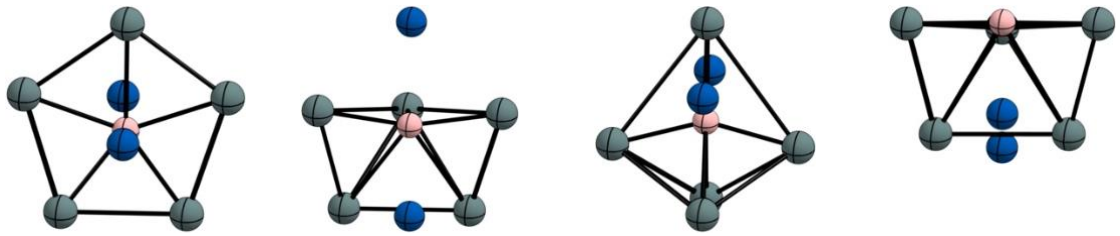

40a
0.0/1.8

40b
1.3/3.5

40c
5.0/6.0

40d
5.4/6.7

Figure S33. Global minimum and low-lying isomers of cluster $BNa_2Sn_5^{-}$. Relative energies are shown in kcal·mol^{-1} at DLPNO-CCSD(T)/CSB//PBE0-D3/def2-TZVP (**in bold**) and PBE0-D3/def2-TZVP levels, including zero-point energy (ZPE) corrections.

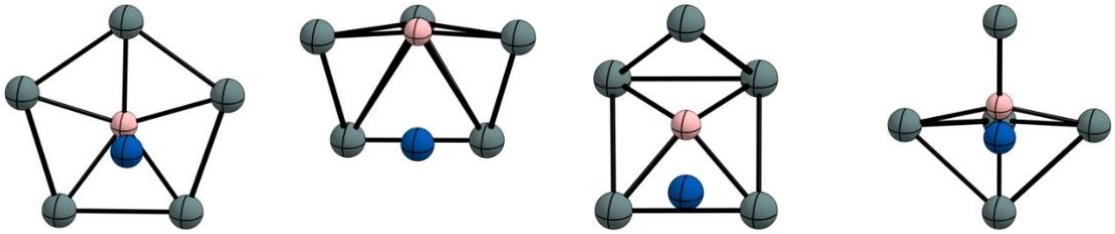

41a **0.0**/0.0 | 41b **0.8**/1.4 | 41b **4.4**/6.3 | 41d **4.6**/6.0

Figure S34. Global minimum and low-lying isomers of cluster $BNaSn_5^{2-}$. Relative energies are shown in kcal·mol^{-1} at DLPNO-CCSD(T)/CSB//PBE0-D3/def2-TZVP (**in bold**) and PBE0-D3/def2-TZVP levels, including zero-point energy (ZPE) corrections.

Table S5. HOMO-LUMO energy gap in eV of the global minimum of BTr_5^{3-} (Tr = Si-Sn) and BTr_4Pn^{2-} (Tr = Si, Ge and Pn = P-Bi) in vacuum at PBE0-D3/def2-TZVP level of theory.

System	E_{HOMO}	E_{LUMO}	ΔE_{H-L}
BSi_5^{3-}	7.2	10.8	3.6
BGe_5^{3-}	7.5	10.9	3.4
BSn_5^{3-}	6.1	8.7	2.5
BSi_4P^{2-}	3.2	6.5	3.3
BSi_4As^{2-}	3.2	6.6	3.4
BGe_4As^{2-}	3.4	6.7	3.3
BSi_4Sb^{2-}	3.0	6.6	3.5
BGe_4Sb^{2-}	2.9	6.4	3.5
BSi_4Bi^{2-}	3.1	6.6	3.6
BGe_4Bi^{2-}	3.1	6.3	3.1

Table S6. HOMO-LUMO energy gap in eV of the global minimum of BTr_5^{3-} (Tr = Si-Sn) and BTr_4Pn^{2-} (Tr = Si, Ge and Pn = P-Bi) in conjunction with the implicit solvent model provided by the Polarizable Continuum Model (PCM) at PBE0-D3/def2-TZVP level of theory.

System	E_{HOMO}	E_{LUMO}	ΔE_{H-L}
BSi_5^{3-}	-3.6	0.1	3.7
BGe_5^{3-}	-3.7	-0.1	3.6
BSn_5^{3-}	-3.1	-0.1	3.0
BSi_4P^{2-}	-4.2	-0.6	3.5
BSi_4As^{2-}	-4.2	-0.7	3.5

BGe_4As^{2-}	-4.1	-0.8	3.3
BSi_4Sb^{2-}	-4.2	-0.8	3.4
BGe_4Sb^{2-}	-4.2	-0.9	3.3
BSi_4Bi^{2-}	-4.2	-0.8	3.4
BGe_4Bi^{2-}	-4.1	-0.9	3.2

Table S7. HOMO-LUMO energy gap in eV for the global minimum of Li_3BTr_5 (Tr = Si-Sn), Li_2BSi_4Pn and Li_2BGe_4Pn (Pn = P-Bi) at PBE0-D3/def2-TZVP level of theory.

System	E_{HOMO}	E_{LUMO}	ΔE_{H-L}
Li_3BSi_5	−4.9	−1.4	3.5
Li_3BGe_5	−4.9	−1.4	3.5
Li_3BSn_5	−4.6	−1.7	2.9
Li_2BSi_4As	−5.7	−1.9	3.8
Li_2BGe_4As	−5.5	−1.7	3.8
Li_2BSi_4P	−5.7	−1.9	3.8
Li_2BSi_4Sb	−5.6	−1.8	3.8
Li_2BGe_4Sb	−5.6	−1.8	3.8
Li_2BSi_4Bi	−5.5	−1.8	3.7
Li_2BGe_4Bi	−5.6	−1.8	3.6

Cartesian Coordinates

Cartesian coordinates of the global minima of BSi_5^{3-}, BGe_5^{3-}, BSn_5^{3-}, BSi_4P^{2-}, BSi_4As^{2-}, BGe_4As^{2-} , BSi_4Sb^{2-}, BGe_4Sb^{2-}, BSi_4Bi^{2-} and BGe_4Bi^{2-} their smallest vibrational frequencies in cm^{-1} at the PBE0- D3/def2-TZVP level.

BSi_5^{3-}
ν_{min} = 177.1

B	0.000000000	0.000000000	0.000000000
Si	0.000000000	2.045634000	0.000000000
Si	-1.945513000	0.632136000	0.000000000
Si	-1.202393000	-1.654952000	0.000000000
Si	1.202393000	-1.654952000	0.000000000
Si	1.945513000	0.632136000	0.000000000

BGe_5^{3-}
ν_{min} = 98.4

B	0.000000000	0.000000000	0.000000000
Ge	0.000000000	2.152078000	0.000000000
Ge	-1.264960000	-1.741068000	0.000000000
Ge	2.046748000	0.665029000	0.000000000
Ge	1.264960000	-1.741068000	0.000000000
Ge	-2.046748000	0.665029000	0.000000000

BSn_5^{3-}
ν_{min} = 56.4

Sn	0.000000000	2.428257000	0.000000000
Sn	1.427294000	-1.964501000	0.000000000
Sn	-1.427294000	-1.964501000	0.000000000
Sn	-2.309410000	0.750373000	0.000000000
B	0.000000000	0.000000000	0.000000000

BSi_4As^{2-}
ν_{min} = 154.1

Si	0.000000000	1.966302000	0.192493000
Si	0.000000000	1.218820000	-2.021441000
Si	0.000000000	-1.218820000	-2.021441000
B	0.000000000	0.000000000	-0.439621000
Si	0.000000000	-1.966302000	0.192493000

Sn	2.309410000	0.750373000	0.000000000	As	0.000000000	0.000000000	1.618444000

BGe_4As^{2-}

ν_{min} = 98.3

Ge	0.000062000	-0.642360000	2.062346000
Ge	0.000062000	-0.642360000	-2.062346000
Ge	0.000062000	1.695108000	1.279777000
Ge	0.000062000	1.695108000	-1.279777000
As	-0.000266000	-2.045505000	0.000000000
B	0.000168000	0.025166000	0.000000000

BSi_4P^{2-}

ν_{min} = 177.1

Si	0.000000000	1.937472000	0.618039000
Si	0.000000000	1.215563000	-1.622512000
Si	0.000000000	-1.215563000	-1.622512000
B	0.000000000	0.000000000	-0.038767000
Si	0.000000000	-1.937472000	0.618039000
P	0.000000000	0.000000000	1.887937000

BSi_4Sb^{2-}

ν_{min} = 136.5

Si	0.000000000	2.005865000	-0.199402000
Si	0.000000000	1.226649000	-2.375578000
Si	0.000000000	-1.226649000	-2.375578000
B	0.000000000	0.000000000	-0.799900000
Si	0.000000000	-2.005865000	-0.199402000
Sb	0.000000000	0.000000000	1.492136000

BGe_4Sb^{2-}

ν_{min} = 85.7

Ge	0.000000000	2.098571000	0.358620000
Ge	0.000000000	-1.289780000	-1.946268000
Sb	0.000000000	0.000000000	2.021109000
Ge	0.000000000	1.289780000	-1.946268000
B	0.000000000	0.000000000	-0.293426000
Ge	0.000000000	-2.098571000	0.358620000

BSi_4Bi^{2-}

ν_{min} = 127.6

Si	0.000000000	2.016692000	-0.600964000
Si	0.000000000	1.232850000	-2.763776000
Si	0.000000000	-1.232850000	-2.763776000
B	0.000000000	0.000000000	-1.191535000
Si	0.000000000	-2.016692000	-0.600964000
Bi	0.000000000	0.000000000	1.206872000

BGe_4Bi^{2-}

ν_{min} = 78.1

Ge	0.000000000	2.108049000	0.009694000
Ge	0.000000000	-1.296269000	-2.280902000
Bi	0.000000000	0.000000000	1.789436000
Ge	0.000000000	1.296269000	-2.280902000
B	0.000000000	0.000000000	-0.633179000
Ge	0.000000000	-2.108049000	0.009694000

References

1. O. Yanez, R. Baez-Grez, D. Inostroza, W. A. Rabanal-Leon, R. Pino-Rios, J. Garza and W. Tiznado, *J. Chem. Theory Comput.*, 2019, **15**, 1463-1475.
2. C. Adamo and V. Barone, *J. Chem. Phys.*, 1999, **110**, 6158-6170.
3. S. Grimme, J. Antony, S. Ehrlich and H. Krieg, *J. Chem. Phys.*, 2010, **132**, 154104.
4. P. Fuentealba, H. Preuss, H. Stoll and L. Von Szentpály, *Chem. Phys. Lett.*, 1982, **89**, 418-422.
5. P. Fuentealba, L. v. Szentpaly, H. Preuss and H. Stoll, *J. Phys. B: Atom. Mol. Phys.*, 1985, **18**, 1287.
6. W. Küchle, M. Dolg, H. Stoll and H. Preuss, *J. Chem. Phys.*, 1994, **100**, 7535-7542.
7. W. Küchle, M. Dolg, H. Stoll and H. Preuss, *Mol. Phys.*, 1991, **74**, 1245-1263.
8. A. Bergner, M. Dolg, W. Küchle, H. Stoll and H. Preuß, *Mol. Phys.*, 1993, **80**, 143-1441.
9. F. Weigend and R. Ahlrichs, *Phys. Chem. Chem. Phys.*, 2005, **7**, 3297-3305.
10. C. Riplinger and F. Neese, *J. Chem. Phys.*, 2013, **138**, 034106.
11. C. Riplinger, P. Pinski, U. Becker, E. F. Valeev and F. Neese, *J. Chem. Phys.*, 2016, **144**, 024109.
12. C. Riplinger, B. Sandhoefer, A. Hansen and F. Neese, *J. Chem. Phys.*, 2013, **139**, 134101.
13. D. G. Truhlar, *Chem. Phys. Lett.*, 1998, **294**, 45-48.
14. F. Neese, A. Hansen and D. G. Liakos, *J. Chem. Phys.*, 2009, **131**, 064103.
15. M. J. Frisch, G. W. Trucks, H. B. Schlegel, G. E. Scuseria, M. A. Robb, J. R. Cheeseman, G. Scalmani, V. Barone, G. A. Petersson, H. Nakatsuji, X. Li, M. Caricato, A. V. Marenich, J. Bloino, B. G. Janesko, R. Gomperts, B. Mennucci, H. P. Hratchian, J. V. Ortiz, A. F. Izmaylov, J. L. Sonnenberg, Williams, F. Ding, F. Lipparini, F. Egidi, J. Goings, B. Peng, A. Petrone, T. Henderson, D. Ranasinghe, V. G. Zakrzewski, J. Gao, N. Rega, G. Zheng, W. Liang, M. Hada, M. Ehara, K. Toyota, R. Fukuda, J. Hasegawa, M. Ishida, T. Nakajima, Y. Honda, O. Kitao, H. Nakai, T. Vreven, K. Throssell, J. A. Montgomery Jr., J. E. Peralta, F. Ogliaro, M. J. Bearpark, J. J. Heyd, E. N.

Brothers, K. N. Kudin, V. N. Staroverov, T. A. Keith, R. Kobayashi, J. Normand, K. Raghavachari, A. P. Rendell, J. C. Burant, S. S. Iyengar, J. Tomasi, M. Cossi, J. M. Millam, M. Klene, C. Adamo, R. Cammi, J. W. Ochterski, R. L. Martin, K. Morokuma, O. Farkas, J. B. Foresman and D. J. Fox, 2016
16. E. D. Glendening, C. R. Landis and F. Weinhold, *J. Comput. Chem.*, 2013, **34**, 1429-1437.
17. D. Y. Zubarev and A. I. Boldyrev, *Phys. Chem. Chem. Phys.*, 2008, **10**, 5207-5217.
18. D. Y. Zubarev and A. I. Boldyrev, *J. Org. Chem.*, 2008, **73**, 925-9258.
19. T. Lu and F. Chen, *J. Comput. Chem.*, 2012, **33**, 580-592.
20. Legault, C. Y. *CYLview20*, Université de Sherbrooke: 2020.
21. W. Humphrey, A. Dalke and K. Schulten, *J. Mol. Graph.*, 1996, **14**, 33-38, 27-38.
22. A. M. n. Pendás, M. A. Blanco and E. Francisco, *J. Chem. Phys.*, 2004, **120**, 458-4592.
23. A. M. Pendás, E. Francisco and M. A. Blanco, *J. Comput. Chem.*, 2005, **26**, 344-351.
24. M. A. Blanco, A. Martín Pendás and E. Francisco, *J. Chem. Theory Comput.*, 2005, **1**, 1096-1109.
25. A. M. Pendás, M. A. Blanco and E. Francisco, *J. Comput. Chem.*, 2007, **28**, 16-184.
26. *T. A. Keith, TK Gristmill Software, Overland Parks, USA, 2019.*
27. G. Monaco, F. F. Summa, R. Zanasi, *J. Chem. Inf. Model.* **2020**, *61*, 270-283.